Cell, *Volume 136*

Supplemental Data

The Ndc80 Kinetochore Complex Forms Load-Bearing Attachments to Dynamic Microtubule Tips via Biased Diffusion

Andrew F. Powers, Andrew D. Franck, Daniel R. Gestaut, Jeremy Cooper, Beth Gracyzk, Ronnie R. Wei, Linda Wordeman, Trisha N. Davis, and Charles L. Asbury

SUPPLEMENTAL DISCUSSION

Uncertainty in the Number of Complexes Required for a Load-Bearing Coupler

We estimated the uncertainty in our calculation of the number of Ndc80 complexes required for load-bearing tip attachment by combining the uncertainties arising from three potential sources of error. First, we used BCA assays (Pierce, Thermo Fisher Scientific, Rockford, IL) to measure the concentrations of our Ndc80 preparations. Based on many replicate measurements, these assays are repeatable to within ± 6% in our hands. The manufacturer additionally reports protein-to-protein variation of ± 15%. Assuming uncorrelated errors, these can be combined (i.e., added in quadrature; Taylor, 1982) to yield a total uncertainty due to protein quantification of ± 16%. The second potential error source is the counting assay used to measure the concentrations of our preparations of anti-His beads. Based on repeated counts, the uncertainty of this measurement is ± 11%. The third source arises from Poisson statistics, which govern the variability in the number of complexes bound to a small area on the bead surface when the binding density is low. In the present case, this source will contribute ± 27% (i.e., $N^{-½}$, where N = 14 is the expected number of bound complexes based on the

average density). Combining all three sources (by adding them in quadrature) yields a total uncertainty of ± 33% or, equivalently, an estimate of 14 ± 5 complexes.

We considered the possibility that Ndc80 complexes might form clusters on the bead surface large enough to significantly increase the number interacting with the filament above our estimate (i.e. clusters > 20 to 30 complexes). However, several observations indicate that such clustering was unlikely. First, beads incubated with ≤ 2 nM GFP-tagged Ndc80 were uniformly decorated and did not exhibit the large bead-to-bead variability in brightness that would occur if the complexes bound in large clusters (Figure S4A and B). Second, their fluorescence increased linearly with the concentration of the complex, which demonstrates an absence of the binding cooperativity that would be expected if clustering were occurring (Figure S4C and D). Third, gel filtration experiments carried out in the same buffer that was used for bead binding showed no evidence for large clusters. The complex elutes as a clean peak with an apparent Stoke's radius close to the predicted size for individual heterotetramers (Figure S1C). Thus the complex does not appear to cluster, either in solution or on the bead surface, under the conditions used here for bead binding.

Estimation of Kinetochore-Microtubule Forces In Vivo

The most straightforward way to estimate the range of forces transmitted to kinetochores during normal movement of bi-oriented chromosomes is to measure the amount of stretching between sister kinetochores and then multiply by the elasticity of the chromatin that links them together. Nicklas (1988) used this method, after determining chromatin elasticity with a calibrated microneedle, to estimate a force of 7 pN per microtubule in meiotic grasshopper spermatocytes. Essentially the same calculation can be performed for budding yeast, yielding a very similar force estimate. Pearson et al. (2001) showed that the pericentric chromatin linking sister kinetochores is extended to

between 0.08 and 0.15 μm kb^{-1}, depending on whether stretching of the lacO GFP marker contributes. A reasonable estimate for the elasticity of this pericentric chromatin is the elasticity measured for chromatin fibers *in vitro*, which varies between 5 and 50 pN kb μm^{-1} depending on histone density (Brower-Toland et al., 2002). Multiplying these values gives the range of forces, 0.4 to 8 pN.

Predictions of the Biased Diffusion Mechanism

Although Hill imagined a sleeve-like coupler completely encircling the microtubule, the physical underpinnings of his model can apply more generally to any array of microtubule binding elements that are linked together. The mechanism he proposed is a form of biased diffusion where the kinetochore undergoes thermally driven movement in a corrugated free energy landscape, as shown schematically in Figure S5A and B. The speed of diffusion depends on the height of the corrugations, which arise because movement along the filament requires breaking some bonds. Moving from one lattice site to another (e.g., from i to ii in Figure S5A and B) results in no net change in energy because the broken bonds can re-form. Thus, lattice-bound couplers in the absence of external load will undergo an unbiased random walk. However, if the coupler begins to move past the tip of the filament (i.e., from ii to iii, where it hangs partially off the end) some binding elements will no longer be able to reach the filament. Thus the free energy increases (in proportion to the number of broken bonds that are unable to re-form), which presents a barrier that biases the diffusion and inhibits detachment. Additionally, the corrugations in the landscape become smaller as the coupler begins to move off the tip because fewer bonds mediate the linkage, so fewer must be broken for further movement. This effect locally increases the rate of diffusion and, as explained in the following paragraph, allows couplers that are nearly immobile on the lattice to track

effectively with shortening tips. Tip tracking requires the diffusion of the coupler to be fast enough and biased enough at the tip to outrun disassembly.

Hill's model predicts several changes in behavior as the number of binding elements changes. The most obvious difference is that couplers with fewer elements are predicted to detach more frequently, owing to their reduced binding energy. Couplers with fewer elements will also diffuse more quickly on the lattice, because fewer bonds must be broken to allow movement. During microtubule shortening, another interesting difference is predicted. Small highly mobile couplers will tend to stay ahead of the disassembling tip by moving randomly on the lattice and only occasionally 'bouncing' off the tip (Figure 7A). Conversely, larger less mobile couplers will track closely with the tip, even if they are so large that their diffusion on the lattice is negligibly slow (Figure 7B). More unidirectional tracking occurs in these cases because the mobility is low on the lattice but increases when the tip begins to disassemble out from under the coupler (see above). This in turn promotes lattice-directed movement and formation of new bonds, resulting in a steady state where the rate of new bond formation is balanced by the loss due to disassembly.

SUPPLEMENTAL EXPERIMENTAL PROCEDURES

Details of Expression Plasmid Construction and Protein Purification

For expression of the *S. cerevisiae* Ndc80 complex, we used two dicistronic vectors encoding the Ndc80/Nuf2 and Spc24/Spc25 sub-complexes that have been described previously (Wei et al., 2005). To create a fluorescent-tagged version of the complex, the Nuf2 gene was excised from one of these vectors and substituted with Nuf2-GFP, which was derived through PCR from yeast strain MSY107-5d (Shimogawa et al., 2006) with

addition of a Spe1 restriction site at the 5' end of the 3' primer. The internal Kpn1 restriction site and Spe1 restriction site were used to ligate the Nuf2-GFP PCR product into the dicistronic vector. For the full-length human Hec1 complex, we created a new polycistronic vector encoding all four subunits. cDNA clones for human Spc25, Spc24 and Hec1 were purchased from ATCC (Manassas, VA), and a clone for human Nuf2 was kindly provided by Jennifer De Luca (Colorado State University). Human Spc25, Spc24, Hec1 and Nuf2 were cloned into cassettes 1, 2, 3, and 4 of the pST39 vector (Tan, 2001) using restriction sites Xba1 & Apa1, EcoR1 & HindIII, EcoRV & Kpn1, and BspE1 & Mlu1, respectively. In addition, a Pac1 site (encoding leucine-isoleucine-asparagine) was added to the 3' end of Spc25 for future cloning. All versions of the complex included a C-terminal His_6-tag on Spc24 to allow affinity purification and bead binding.

Vectors were transformed into *E. coli* BL21 (Rosetta; Novagen, Madison, WI) and protein expression and purification were carried out as previously described (Asbury et al., 2006; Franck et al., 2007; Gestaut et al., 2008). Cells containing the target plasmid(s) were grown at 37° C until they reached a density of 30 Klett units, induced overnight (~12 hours) at 23° C with the addition of 0.2 mM IPTG, then pelleted. Fresh pellets were lysed using a French press in 50 mM HEPES (pH 7.6) containing 300 mM NaCl, 2.5 U mL^{-1} benzonase, and protease inhibitors (0.01 mg mL^{-1} chymostatin, 0.01 mg mL^{-1} aprotinin, 0.01 mg mL^{-1} leupeptin, 0.01 mg mL^{-1} pepstatin, 0.002 mg mL^{-1} benzamadine and 1 mM phenylmethylsulfonyl fluoride) and clarified by centrifugation. Protein was purified by affinity chromatography using TALON resin as described by the manufacturer (BD Biosciences). Peak elutions were concentrated using an Amicon Ultra 50 kD MWCO centrifugal filter (Millipore, Billerica, MA) and then subjected to gel filtration chromatography on an SDX200 16/60 (GE Healthcare, Pistcataway, NJ) equilibrated

with 50 mM HEPES (pH 7.6) containing 200 mM NaCl. Glycerol was added to a final concentration of 10% and aliquots were snap frozen and stored at -80˚ C.

SUPPLEMENTAL REFERENCES

Brower-Toland, B. D., Smith, C. L., Yeh, R. C., Lis, J. T., Peterson, C. L., and Wang, M. D. (2002). Mechanical disruption of individual nucleosomes reveals a reversible multistage release of DNA. Proc Natl Acad Sci U S A *99*, 1960-1965.

Gestaut, D. R., Graczyk, B., Cooper, J., Widlund, P. O., Zelter, A., Wordeman, L., Asbury, C. L., and Davis, T. N. (2008). Phosphoregulation and depolymerization-driven movement of the Dam1 complex do not require ring formation. Nat Cell Biol *10*, 407-414.

Hill, T. L. (1985). Theoretical problems related to the attachment of microtubules to kinetochores. Proc Natl Acad Sci U S A *82*, 4404-4408.

Nicklas, R. B. (1988). The forces that move chromosomes in mitosis. Annu Rev Biophys Biophys Chem *17*, 431-449.

Pearson, C. G., Maddox, P. S., Salmon, E. D., and Bloom, K. (2001). Budding yeast chromosome structure and dynamics during mitosis. J Cell Biol *152*, 1255-1266.

Shimogawa, M. M., Graczyk, B., Gardner, M. K., Francis, S. E., White, E. A., Ess, M., Molk, J. N., Ruse, C., Niessen, S., Yates, J. R., 3rd*, et al.* (2006). Mps1 phosphorylation of Dam1 couples kinetochores to microtubule plus ends at metaphase. Curr Biol *16*, 1489-1501.

Tan, S. (2001). A modular polycistronic expression system for overexpressing protein complexes in Escherichia coli. Protein Expr Purif *21*, 224-234.

Taylor, J. R. (1982). An introduction to error analysis : the study of uncertainties in physical measurements (Mill Valley, CA: University Science Books).

Wei, R. R., Sorger, P. K., and Harrison, S. C. (2005). Molecular organization of the Ndc80 complex, an essential kinetochore component. Proc Natl Acad Sci U S A *102*, 5363-5367.

SUPPLEMENTAL TABLE AND FIGURES

Table S1. Outcomes during Force-Clamp Experiments with Yeast or Human Ndc80 Complex, under 0.5 to 2.5 pN of Continuous Tension

		yeast Ndc80 complex	human Ndc80/Hec1 complex
A	total events observed	392	50
B	events with discernable assembly-coupled movement only	250 (64%)[1]	25 (50%)[1]
C	events with both assembly- and disassembly-coupled movement	64 (16%)[1]	21 (42%)[1]
D	events with discernable disassembly-coupled movement only	78 (20%)[1]	4 (8%)[1]
E	total events with discernable assembly-coupled movement (B+C)	314	46
F	'catastrophes' during assembly-coupled movement	64 (20%)[2]	21 (45%)[2]
G	detachments during assembly-coupled movement	226 (72%)[2]	15 (33%)[2]
H	other interruptions to assembly-coupled movement	24 (8%)[2]	10 (22%)[2]
I	total events with discernable disassembly-coupled movement (C+D)	142	25
J	'rescues' during disassembly-coupled movement	4 (3%)[3]	2 (8%)[3]
K	detachments during disassembly-coupled movement	83 (58%)[3]	23 (92%)[3]
L	other interruptions to disassembly-coupled movement	55 (39%)[3]	0 (0%)[3]

[1] expressed as a percentage of total events (row A)
[2] expressed as a percentage of total events with discernable assembly-coupled movement (row E)
[3] expressed as a percentage of total events with discernable disassembly-coupled movement (row I)

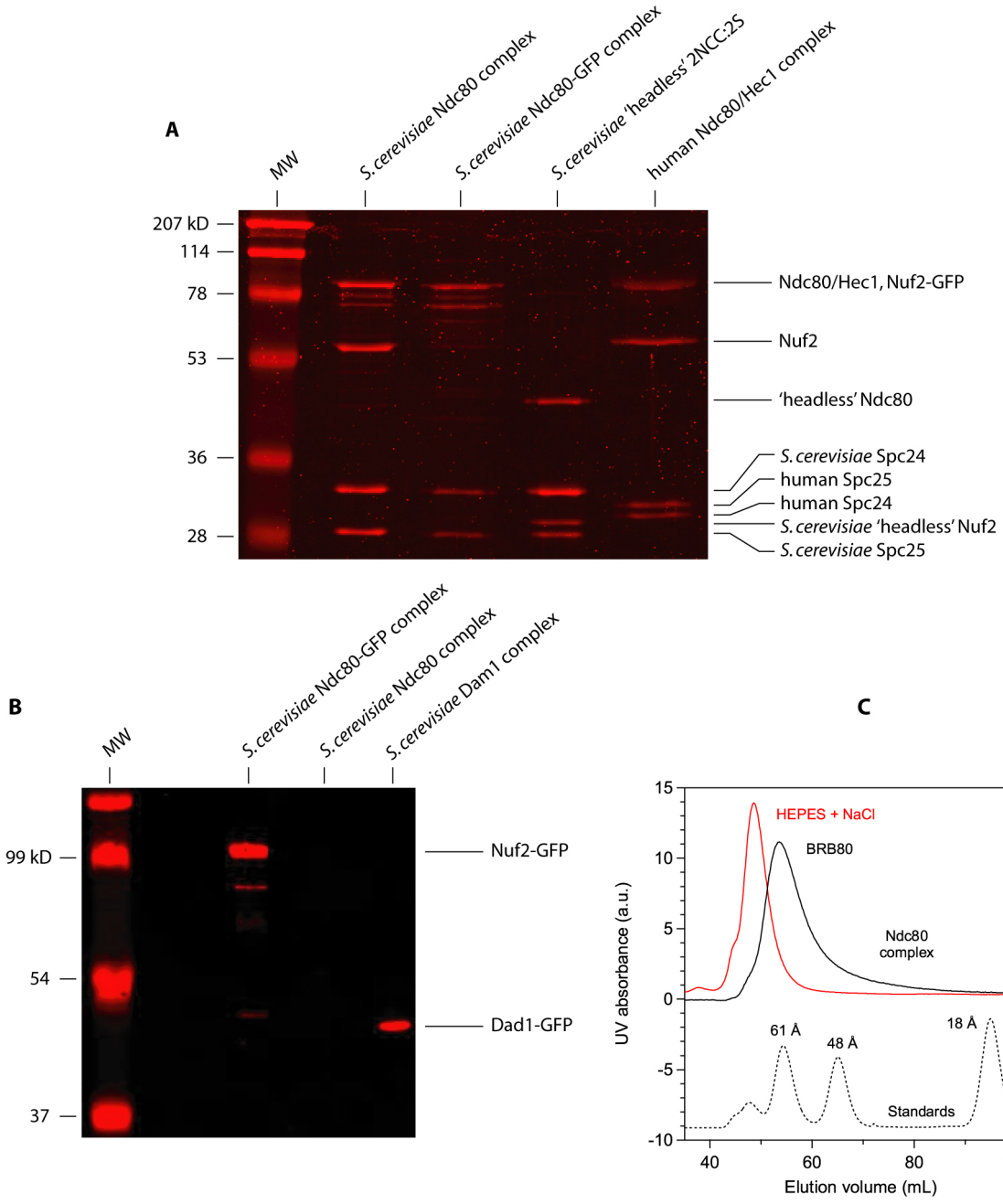

Figure S1. Purification of the Ndc80 complex

(A) Coommassie stained SDS-PAGE (12% acrylamide) showing the components of the *S. cerevisiae* Ndc80 complex, the GFP-tagged *S. cerevisiae* Ndc80 complex, the 'headless' 2NCC:2S complex and the human Ndc80/Hec1 complex.

(B) Anti-GFP Western blot showing the GFP-tagged Nuf2 subunit of the *S. cerevisiae* Ndc80 complex. As negative and positive controls, untagged Ndc80 complex and GFP-tagged Dam1 complex (Gestaut et al., 2008) were run in adjacent lanes.

(C) Gel filtration profile for the yeast Ndc80 complex in our standard purification buffer (50 mM HEPES pH 7.6 plus 300 mM NaCl; red trace) and in the buffer used for binding the complex to anti-His beads (BRB80; solid black trace). For comparison, the elution profile for a mixture of standard proteins in purification buffer is also shown (ferritin, Stoke's radius of 61 angstroms; aldolase, 48 angstroms; RNAse, 18 angstroms; dotted black trace, offset vertically for clarity).

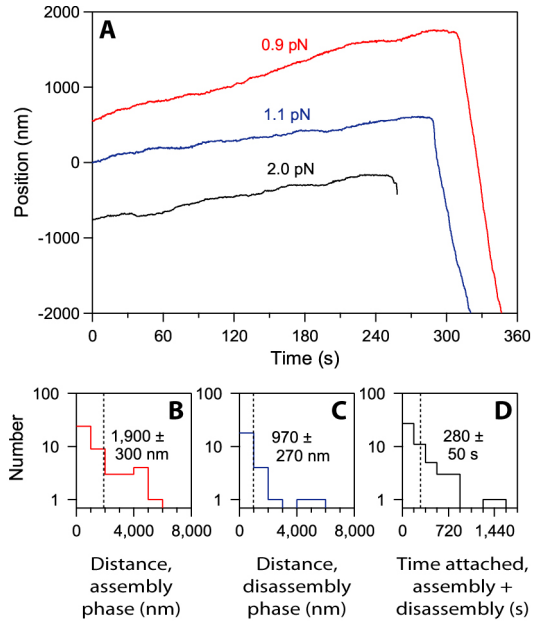

Figure S2. The human Ndc80/Hec1 complex couples force to dynamic microtubule tips
(A) Beads coated with the human Ndc80/Hec1 complex form persistent load-bearing attachments to growing and shortening microtubule tips, similar to attachments formed by the yeast Ndc80 complex. Records show bead position versus time during continuous application of tensile load, as in Figure 2A.
(B – D) Histograms of distance moved during assembly (N = 46 records), distance moved during disassembly (N = 25), and total attached time (including both assembly and disassembly phases; N = 50) for tip-attached beads moving under 0.5 - 2.5 pN of tension. Dotted vertical lines indicate the average for each distribution. Uncertainties represent s.e.m.

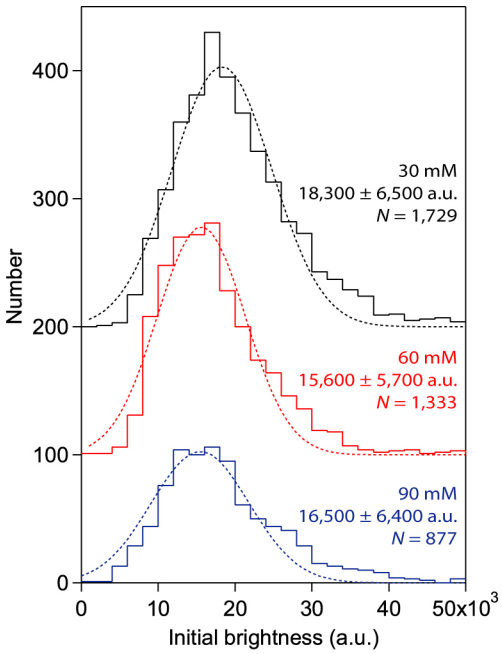

Figure S3. The brightness of diffusing Ndc80-GFP spots is unaffected by ionic strength
Distributions of initial brightness values for Ndc80-GFP particles diffusing on taxol-stabilized microtubules in 30 mM K^+ (black), 60 mM K^+ (red) or 90 mM K^+ (blue) buffer. Each histogram was fit by a Gaussian function (dotted lines) to determine the mean brightness values indicated. Uncertainties represent s.d. For clarity, the 60 mM K^+ and 90 mM K^+ distributions are offset vertically by 100 and 200 counts, respectively.

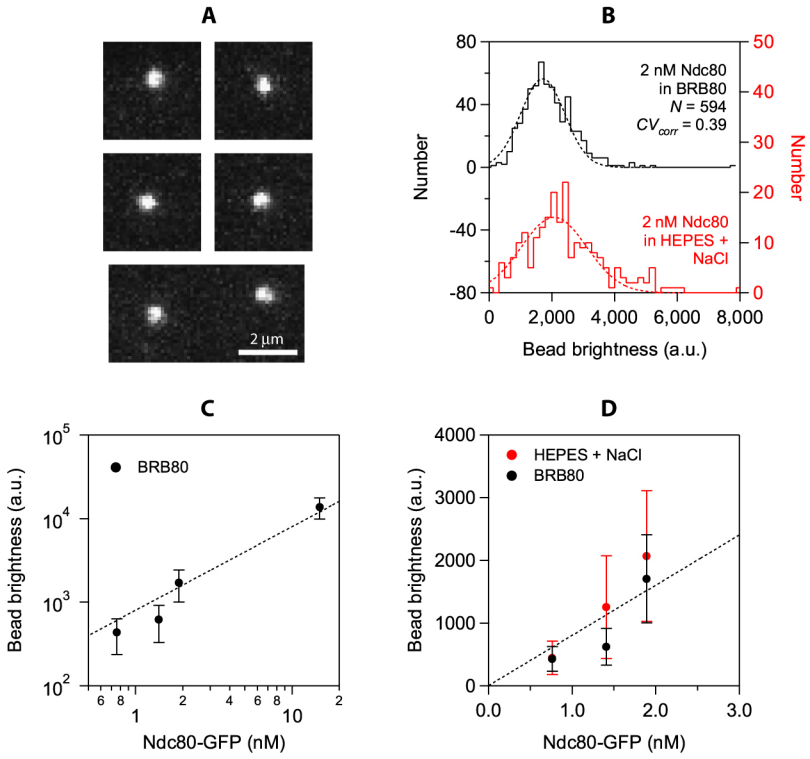

Figure S4. Quantification of GFP-tagged Ndc80 complex bound to anti-His beads
(A) Epifluorescence images of anti-His beads after incubation with 2 nM GFP-tagged Ndc80 complex in our standard binding buffer (BRB80 plus 8 mg mL^{-1} BSA and 1 mM DTT).
(B) Brightness distributions for beads incubated with 2 nM GFP-tagged Ndc80 complex in our standard binding buffer (black histogram) or in the buffer used for purification of the complex (50 mM HEPES pH 7.6 plus 300 mM NaCl; red histogram).
(C and D) Mean brightness for beads incubated with GFP-tagged Ndc80 in our standard binding buffer (black symbols) or in purification buffer (red symbols) plotted against the concentration of the complex. Uncertainties represent s.d. The bead concentration was 5.6 pM for all incubations.

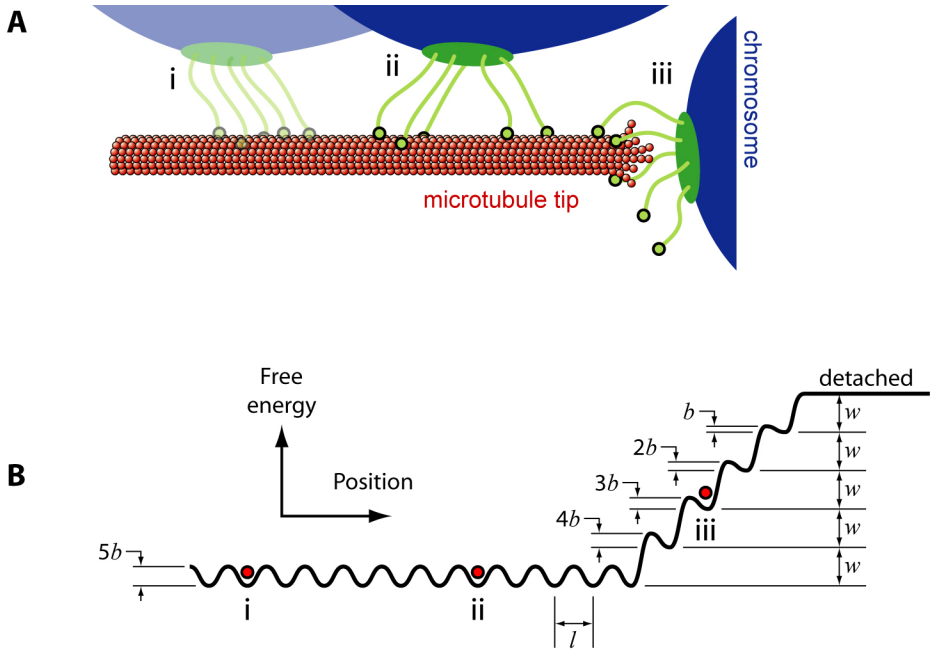

Figure S5. The biased diffusion model

(A) Schematic picture of a coupler composed of five microtubule binding elements attached to a microtubule at three different locations, two on the lattice (denoted i and ii) and one on the tip in a position where two of the elements are no longer bound (iii).

(B) Free energy landscape for a five-element, biased diffusion-based coupler. The spacing of sites is denoted by l. The gradual increase in free energy on the right arises from the bond energies, w, that must be overcome to move the coupler past the filament tip. The corrugations in the landscape occur because movement along the filament requires breaking and reforming some bonds. Their heights, $5b, 4b, ..., b$, decrease as the coupler begins to move past the tip. Red circles (i, ii, and iii) denote the landscape positions corresponding to the couplers shown in (A).